



Magnetic field dependence of the magnon spin diffusion length in the magnetic insulator yttrium iron garnet

L. J. Cornelissen* and B. J. van Wees

Physics of Nanodevices, Zernike Institute for Advanced Materials, University of Groningen, Nijenborgh 4, 9747 AG Groningen, The Netherlands

(Received 4 December 2015; published 19 January 2016)

We investigated the effect of an external magnetic field on the diffusive spin transport by magnons in the magnetic insulator $\text{Y}_3\text{Fe}_5\text{O}_{12}$, using a nonlocal magnon transport measurement geometry. We observed a decrease in magnon spin diffusion length λ_m for increasing field strengths, where λ_m is reduced from $9.6 \pm 1.2 \mu\text{m}$ at 10 mT to $4.2 \pm 0.6 \mu\text{m}$ at 3.5 T at room temperature. In addition, we find that there must be at least one additional transport parameter that depends on the external magnetic field. Our results do not allow us to unambiguously determine whether this is the magnon equilibrium density or the magnon diffusion constant. These results are significant for experiments in the more conventional longitudinal spin Seebeck geometry, since the magnon spin diffusion length sets the length scale for the spin Seebeck effect as well and is relevant for its understanding.

DOI: [10.1103/PhysRevB.93.020403](https://doi.org/10.1103/PhysRevB.93.020403)

The magnetic insulator yttrium iron garnet (YIG) provides an ideal platform for the study of spin waves [1], due to its low magnetic damping [2] and the fact that no electronic currents can flow in this material. It has been shown that spin waves in the gigahertz regime can be transported through YIG waveguides over large distances [3,4]. Recently, research efforts are also directed to the high-frequency part of the spin wave spectrum, studying the diffusive transport of quantized spin waves (magnons). This has been largely motivated by the observation of the spin Seebeck effect (SSE) in YIG by Uchida *et al.* [5], in which a magnon current is generated by applying a temperature gradient over the magnetic insulator. This temperature gradient results in excitation and diffusion of thermal magnons, which can result in thermal spin pumping when the magnetic insulator is coupled to a normal metal layer [6]. Very recently it has been shown that these thermal magnons can also be excited electrically, and can transport spin through YIG. Their transport can be described diffusively, characterized by the magnon spin diffusion length λ_m , the length scale over which the magnon spin current decays exponentially [7].

The SSE in YIG has been studied extensively, both theoretically [6,8–10] and experimentally [11–18]. Recent experiments show that the voltage resulting from the SSE is reduced upon increasing the external magnetic field [13,14,19]. A mechanism in which low-frequency magnons contribute more to the SSE than high-frequency ones has been proposed to explain these results. The magnetic field will open a Zeeman gap in the magnon density of states, thus “freezing out” the low-frequency magnons with energies below the gap. This could then cause the reduction in SSE signal.

In this Rapid Communication we investigate the effect of the applied magnetic field on the diffusive transport of magnon spins. We employ a nonlocal measurement geometry in which we measure the magnon spin signal as a function of distance, which allows us to directly extract the magnon spin diffusion length for various magnetic field strengths.

The main advantage of this method is that the locations of both magnon injection and detection are well determined, due to the localized magnon injection and detection resulting from the exchange interaction between a spin accumulation in the platinum injector/detector and magnons in the YIG. This means that the distance over which the magnon spin current diffuses is known precisely. Our results clearly indicate that the magnon spin diffusion length decreases for increasing magnetic field strength, causing a strong reduction of the magnon spin signal.

The measurement geometry is shown schematically in Fig. 1 and is equivalent to the nonlocal geometry we developed in Ref. [7]. The platinum injector and detector are placed a distance d apart. We measured two series of samples, series A and series B, tailored to perform measurements in the short ($d \sim 0.2\text{--}5 \mu\text{m}$) and long ($d \sim 2.5\text{--}30 \mu\text{m}$) separation distance regime, respectively. Our samples consist of a (111) single crystal $\text{Y}_3\text{Fe}_5\text{O}_{12}$ film with a thickness of 200 nm (series A) or 210 nm (series B) grown on a 500- μm thick (111) $\text{Gd}_3\text{Ga}_5\text{O}_{12}$ substrate by liquid-phase epitaxy. The YIG samples were provided by the Université de Bretagne Occidentale in Brest, France (series A) and obtained commercially from Matesy GmbH (series B). We define the platinum injector and detector strips on top of the YIG film using three steps of electron beam lithography. The first step results in a pattern of Ti/Au markers, used to align the following steps. In the second step, we define the platinum injector and detector, which are deposited by dc sputtering in an Ar^+ plasma. The platinum thickness is approximately 13.5 and 7 nm, for series A and B, respectively. In the final step we define Ti/Au (5/75 nm) contacts and bonding pads using electron beam evaporation. Prior to the titanium evaporation, argon ion milling was performed to remove polymer residues from the platinum strips. The platinum injector and detector dimensions are $w^A = 100\text{--}150 \text{ nm}$, $w^B = 300 \text{ nm}$, $L^A = 12.5 \mu\text{m}$, and $L^B = 100 \mu\text{m}$, where w and L denote strip width and length, respectively.

We perform a nonlocal measurement by applying a current I (typically $I_{\text{rms}} = 200 \mu\text{A}$) to the injector. Due to the spin Hall effect, this generates a spin current towards the YIG, resulting in a spin accumulation at the YIG|Pt interface. Depending on

*l.j.cornelissen@rug.nl

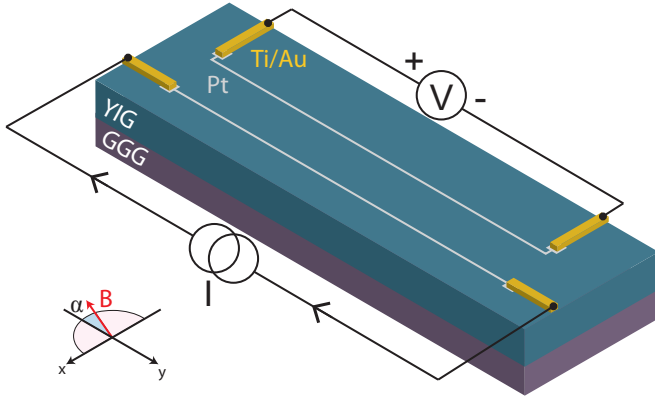


FIG. 1. Schematic of our typical device geometry. The platinum injector and detector strips are contacted by Ti/Au leads, and current (I) and voltage (V) connections are indicated. The magnetic field is rotated in the xy plane (the plane of the sample surface), making an angle α with the negative y axis.

the orientation of the spin accumulation with respect to the YIG magnetization, magnons will be generated in the YIG. These magnons will diffuse to the detector, where they are absorbed and generate a spin current into the platinum, which by virtue of the inverse spin Hall effect will be converted to a charge voltage V (in an open circuit geometry), as shown in Refs. [7,20]. The nonlocal resistance is now defined as $R^{n\omega} = V/I^n$ and is a measure for the magnitude of the magnon spin current between injector and detector. Using a lock-in detection technique [17], we are able to separately detect the first-harmonic ($n = 1$) and second-harmonic ($n = 2$) response of the sample to our excitation frequency $\omega = 2\pi f$, allowing us to separately probe the physics of magnons that are excited electrically [7,20] and thermally [7,11], respectively.

We then rotate the sample in an external field, thereby varying the angle between the YIG magnetization and the spin accumulation in the injector. When $\alpha = 0$, the magnetization is parallel to the charge current in the injector, hence perpendicular to the spin accumulation and no magnons are excited or detected. When $\alpha = \pm 90$ degrees, spin accumulation and

magnetization are collinear and the magnon generation and detection efficiency is maximal. The magnitude of the external field is varied, ranging from 10 mT to 7 T. A typical measurement result (for $d = 2.5 \mu\text{m}$) is shown in Fig. 2, for both the first-harmonic [Fig. 2(a)] and second-harmonic [Fig. 2(b)] response.

For electrically excited magnons, both injection efficiency η_{inj} and detection efficiency η_{det} depend on the angle α as $\eta_{\text{inj}}, \eta_{\text{det}} \propto \sin \alpha$. Since the total signal is then proportional to the product of η_{inj} and η_{det} , this results in a total angular dependence of $R^{1\omega} = R_{\text{nl}}^{1\omega} \sin^2 \alpha$, where $R_{\text{nl}}^{1\omega}$ is the amplitude of the first-harmonic signal [7] [indicated in Fig. 2(a)]. The second-harmonic signal, however, relies on the magnon spin current generated by the spin Seebeck effect in the YIG, due to the temperature gradient arising from Joule heating in the injector. Since Joule heating is independent of α , the only angular dependence for the second-harmonic nonlocal signal comes from the magnon detection efficiency η_{det} , resulting in $R^{2\omega} = R_{\text{nl}}^{2\omega} \sin \alpha$, where $R_{\text{nl}}^{2\omega}$ is the amplitude of the second-harmonic signal [7] [indicated in Fig. 2(b)]. From Fig. 2 we can clearly see that both the first- and second-harmonic signals decrease for increasing external field strengths.

In order to investigate the dependence of the nonlocal signals on the magnetic field, we performed a series of nonlocal measurements as a function of field strength for various injector-detector separation distances. The results are shown in Fig. 3, presenting the data for the first-harmonic signal on the left [Fig. 3(a)] and the second-harmonic signal on the right [Fig. 3(b)]. The distances that we measured are 200 nm, 1 μm , 2.5 μm , 5 μm , 15 μm , 20 μm , and 30 μm . The devices with $d = 200$ nm and $d = 1 \mu\text{m}$ are in sample series A, the other distances in series B.

For both first- and second-harmonic results, it can be seen that the signal at larger distances is suppressed much more strongly by the external field than at shorter distances. In particular, for the first-harmonic response, at $d = 30 \mu\text{m}$ the signal is reduced to ≈ 0 for a field of 1 T, whereas for $d = 200$ nm there is virtually no signal reduction up to approximately 1.5 T. For the intermediate distance $d = 2.5 \mu\text{m}$ the signal is suppressed for a field of 1 T, but only by 24%

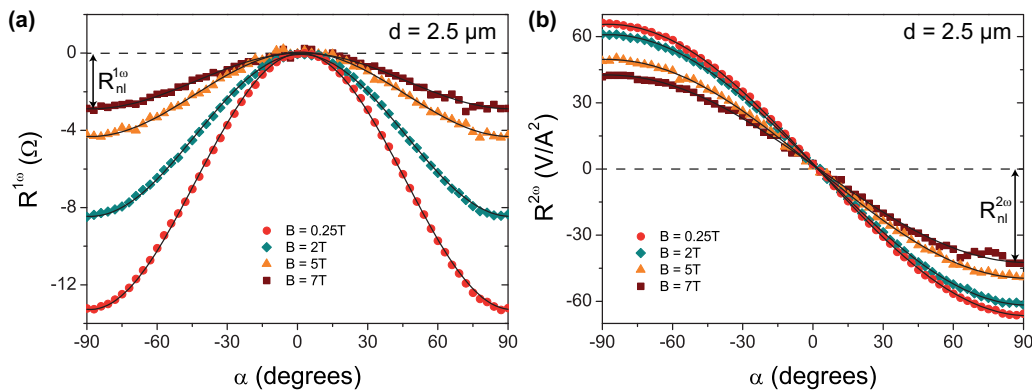


FIG. 2. Nonlocal signal as a function of angle α , for an injector-detector separation distance $d = 2.5 \mu\text{m}$ and for various external magnetic field strengths. (a) First-harmonic signal. The solid lines are $\sin^2 \alpha$ fits through the data. (b) Second-harmonic signal. The solid lines are $\sin \alpha$ fits through the data. The decrease in signal amplitude for increasing magnetic field strength is clearly visible for both first- and second-harmonic signals. The amplitudes of the nonlocal signals, $R_{\text{nl}}^{1\omega}$ and $R_{\text{nl}}^{2\omega}$, are indicated in (a) and (b), respectively, for $B = 7$ T. These measurements were performed using $I_{\text{rms}} = 110 \mu\text{A}$ at a lock-in frequency of $f = 10.447$ Hz.

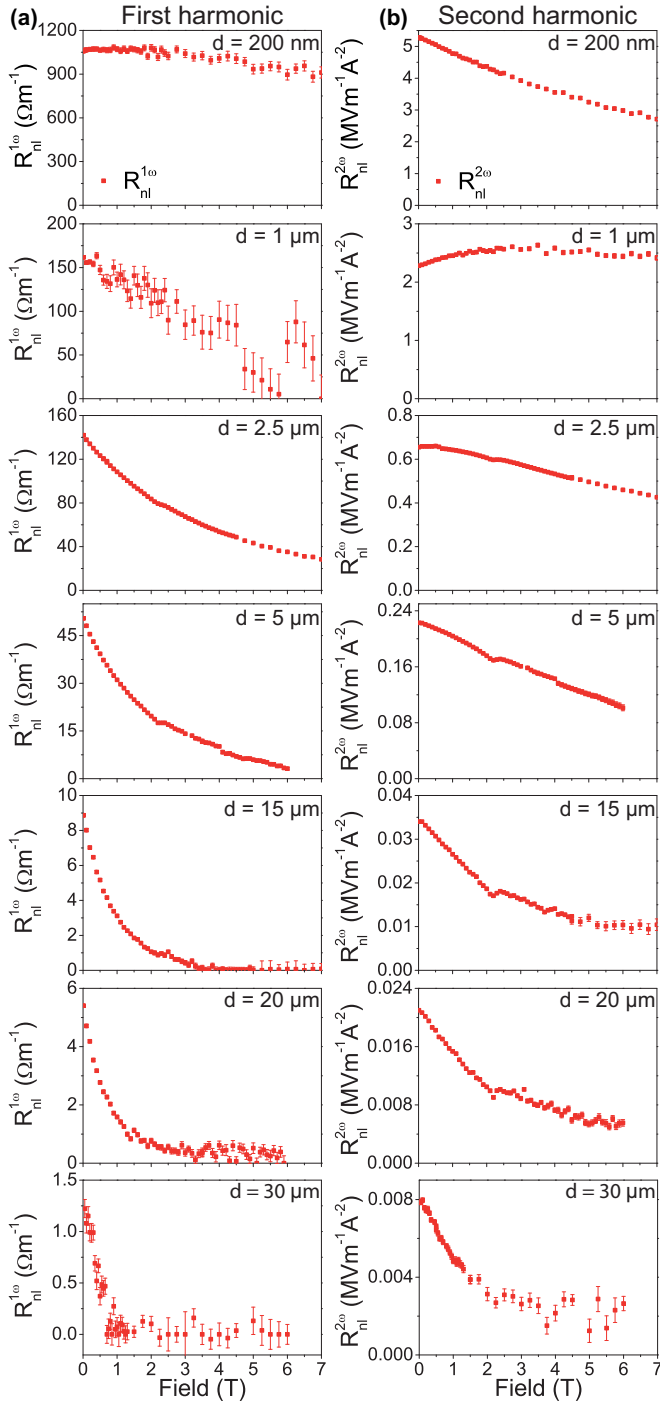


FIG. 3. Magnitude of the first- (a) and second- (b) harmonic nonlocal signals (normalized to device length) as a function of magnetic field, for injector-detector separation distances $d = 200$ nm to $d = 30$ μm . In each plot, the red squares mark the amplitude of the signal, extracted from an angle-dependent measurement as shown in Fig. 2. The error bars represent the standard error in the fit to extract the amplitude. All measurements were performed at an excitation current of $I_{\text{rms}} = 200$ μA with frequency $f = 10.447$ Hz. The data shows structure at $B \approx 2.2$ T which reproduces for distances $d > 2.5$ μm in both the first- and second-harmonic signal. At this moment, the origin of this structure is unclear.

(compared to the signal at 10 mT). These observations clearly indicate that the mechanism leading to signal suppression must

lie in the magnon transport rather than in the generation or detection of magnons: A reduction in η_{inj} or η_{det} would lead to the same signal suppression at all distances.

As we derived in Ref. [7], the nonlocal resistance as a function of injector-detector separation distance is given by

$$R_{\text{nl}} = \frac{C}{\lambda_m} \frac{\exp(d/\lambda_m)}{1 - \exp(2d/\lambda_m)}, \quad (1)$$

where d is the distance between injector and detector and C is a distance independent prefactor that depends, for instance, on the effective spin mixing conductance of the Pt|YIG interface and the magnon diffusion constant D_m . Furthermore, $\lambda_m = \sqrt{D_m \tau}$ is the magnon spin diffusion length, where τ is the magnon spin relaxation time. From Eq. (1) it becomes apparent that for $d > \lambda_m$ a slight reduction of λ_m can cause a large drop in R_{nl} , while as long as $d \ll \lambda_m$ the nonlocal resistance is (in first-order approximation) equal to $-C/(2d)$ and hence the signal will not be influenced by a change in λ_m . The behavior observed in the data shown in Fig. 3 can therefore be explained by assuming that λ_m is not a constant, yet is reduced under the influence of the external field.

In order to assess the field dependency of λ_m , we plot the data presented in Fig. 3 as a function of distance, for various magnetic field strengths. This allows us to extract λ_m at each field value, by fitting the distance-dependent data to Eq. (1). The results of this procedure are shown in Figs. 4(a) and 4(b) for the first- and second-harmonic signals, respectively. The solid lines are fits through the data to Eq. (1), which are performed with weights $w_i \propto 1/y_i^2$, where y_i is the amplitude of data point i , thus giving more weight to data points at large distances (which have a smaller amplitude but contain more information about λ_m compared to the points at short distances). It can be seen from the figure that for both the first and second harmonic, the slope of the fit (in the region $d > 5$ μm) changes for increasing field strength, indicating a decrease of λ_m . The shaded regions in the plots represent the noise floor in our measurement setup, which is approximately 4 nV_{rms}. We perform a fit of Eq. (1) to the data up to $B = 3.5$ T since the signal has dropped below the noise floor at that field value for distances $d \geq 15$ μm , which leaves us with insufficient data points to unambiguously extract λ_m for larger field values. The same procedure is used for the second-harmonic data presented in Fig. 4(b), where in this case we can perform the fits up to $B = 6.0$ T due to the larger signal-to-noise ratio for the second-harmonic signal.

From the fits shown in Fig. 4 we find the magnon spin diffusion length as a function of field, $\lambda_m(B)$, which we plotted in Fig. 5(a). In this figure, both the spin diffusion length extracted from the first-harmonic and second-harmonic signals ($\lambda^{1\omega}$ and $\lambda^{2\omega}$, respectively) are shown. For fields up to $B = 0.7$ T, the spin diffusion lengths extracted from the first- and second-harmonic signals are equal within the measurement uncertainty. For larger fields, however, $\lambda^{1\omega}$ saturates to a smaller value than $\lambda^{2\omega}$. This corresponds to the smaller change in slope of the fits when comparing the distance dependence of the second-harmonic signal in Fig. 4(b) to that of the first harmonic in Fig. 4(a). This is due to the fact that while the first-harmonic signal truly drops to zero for large fields (see Fig. 3(a) for $d \geq 15$ μm), the second-harmonic signal saturates at a finite value even for very

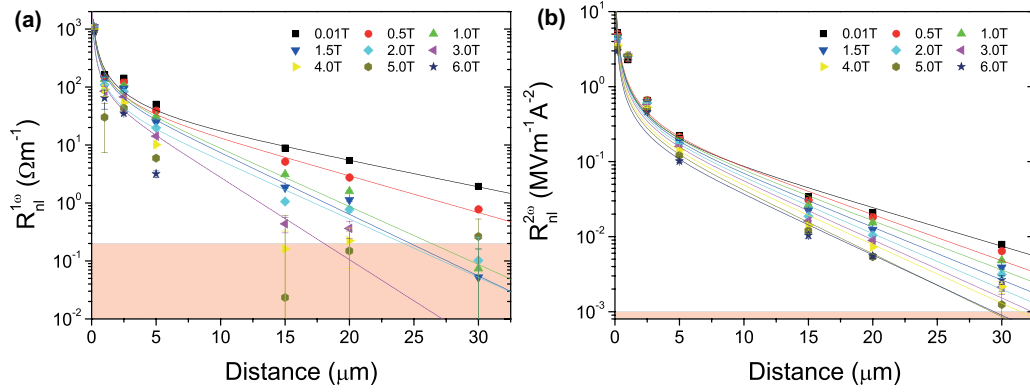


FIG. 4. Data presented in Fig. 3, plotted as a function of distance for the first- (a) and second- (b) harmonic nonlocal signals (normalized to device length), for magnetic field strengths of $B = 0.01$ T to $B = 6.0$ T. In each plot, the symbols mark the amplitude of the signal, extracted from an angle-dependent measurement as shown in Fig. 2. The error bars represent the standard error in the fit to extract the amplitude. The solid lines are fits of Eq. (1) through the data. The shaded regions on the bottom of the graphs indicate the noise floor of the setup for our measurement settings.

large field and distance (see Fig. 3(b), for instance $d = 30 \mu\text{m}$). This finite saturation value might be due to a local heating effect: While at large fields the magnons generated near the injector cannot reach the detector anymore due to the short spin diffusion length, a small temperature gradient (resulting from injector Joule heating) could very well still be present near the detector. This temperature gradient would then give rise to a spin Seebeck voltage as it generates magnons locally, meaning that no spin information, but only heat, is transported from injector to detector. This theory could be tested quantitatively by performing detailed finite element modeling of our devices, which would be interesting but is beyond the scope of this current Rapid Communication.

Another indication that the situation for the thermally excited magnons is more complicated comes from the fact that for $d = 1 \mu\text{m}$ the second-harmonic signal slightly increases up to a field of 2.5 T, rather than immediately decreasing as is observed for all other distances. We do not have an explanation for this behavior at this moment.

Finally, from the data for $d = 200$ nm it is clear that the nonlocal signal is reduced for large fields, despite the fact that $d \ll \lambda_m$ which should imply that R_{nl} is independent of λ_m . Specifically, a reduction of λ_m from 9.5 to 4 μm , as shown in Fig. 5(a), should result in a signal reduction of only

0.03% at $d = 200$ nm. The observed signal reduction for this distance is 3% (from $B = 10$ mT to 3.5 T), which is thus too large to be explained only by a reduction of λ_m . This can be understood by realizing that the prefactor C is also reduced under the influence of the magnetic field, as shown in Fig. 5(b). Comparing the situation for a magnetic field of 10 mT and 3.5 T, both $\lambda_m^{1\omega}$ and $C^{1\omega}$ are reduced by a factor of 0.44. Since $C^{1\omega}$ depends linearly on D_m , we might assume that the reduction of $C^{1\omega}$ can be explained by a reduction of D_m by this same factor. However, since we have that $\lambda_m = \sqrt{D_m \tau}$, this means that τ also has to decrease as a function of the magnetic field in order to explain the observed change in λ_m . However, the equilibrium magnon density n also influences C , so the effect we observed might also be explained by a reduction of n as proposed in Refs. [13,14].

Summarizing, we have investigated the influence of an external magnetic field on the diffusive transport of magnon spins in YIG. The most important effect that we found is that the magnon spin diffusion length reduces as a function of field, decreasing from $\lambda_m = 9.6 \pm 1.2 \mu\text{m}$ at 10 mT to $\lambda_m = 4.2 \pm 0.6 \mu\text{m}$ at 3.5 T at room temperature. For field values higher than 3.5 T, we cannot extract λ_m reliably since the signals at long distances drop below the noise floor for those fields. We also found that for thermally generated magnons,

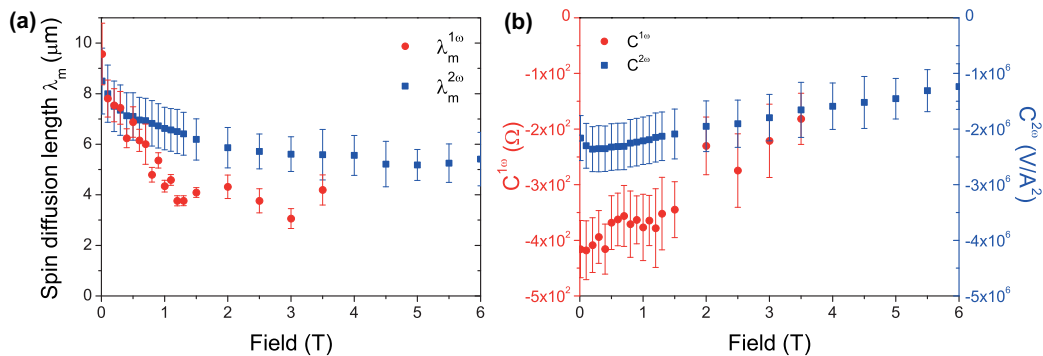


FIG. 5. (a) Magnon spin diffusion length λ_m as a function of external magnetic field, extracted from a fit of Eq. (1) to the distance dependence of the first-harmonic (red circles) and second-harmonic (blue squares) signals. (b) Prefactor C as a function of external magnetic field, extracted from the first (red circles, left axis) and second (blue squares, right axis) harmonic signals.

λ_m appears to saturate at a higher value than for electrically generated ones. We postulate that this might be due to the presence of a small but finite local contribution to the SSE at the detector, arising from diffusion of the heat generated at the injector. This implies that for large fields, we can no longer rely on the second-harmonic signal to extract λ_m . Furthermore, we showed that the observed signal reduction cannot be explained solely by the suppression of λ_m , but requires an additional transport parameter to be field dependent. From the data presented here we cannot identify whether this parameter is the magnon diffusion constant D_m or the equilibrium magnon density n . However, it is clear that the observed magnetic

field dependence of the magnon spin diffusion length needs to be taken into account in the analysis of the magnetic field dependence of the spin Seebeck effect.

The authors would like to acknowledge H. M. de Roosz, J. G. Holstein, H. Adema, and T. J. Schouten for technical assistance, J. Ben Youssef for providing the YIG film used in the fabrication of sample series A. and R. A. Duine for discussions. This work is part of the research program of the Foundation for Fundamental Research on Matter (FOM) and supported by NanoLab NL, EU-FET Grant No. 612759 InSpin and the Zernike Institute for Advanced Materials.

-
- [1] A. A. Serga, A. V. Chumak, and B. Hillebrands, *J. Phys. D: Appl. Phys.* **43**, 264002 (2010).
- [2] V. V. Kruglyak, S. O. Demokritov, and D. Grundler, *J. Phys. D: Appl. Phys.* **43**, 264001 (2010).
- [3] A. V. Chumak, A. A. Serga, M. B. Jungfleisch, R. Neb, D. A. Bozhko, V. S. Tiberkevich, and B. Hillebrands, *Appl. Phys. Lett.* **100**, 082405 (2012).
- [4] A. V. Chumak, V. I. Vasyuchka, A. A. Serga, and B. Hillebrands, *Nat. Phys.* **11**, 453 (2015).
- [5] K. Uchida, J. Xiao, H. Adachi, J. Ohe, S. Takahashi, J. Ieda, T. Ota, Y. Kajiwara, H. Umezawa, H. Kawai *et al.*, *Nat. Mater.* **9**, 894 (2010).
- [6] J. Xiao, G. E. W. Bauer, K.-i. Uchida, E. Saitoh, and S. Maekawa, *Phys. Rev. B* **81**, 214418 (2010).
- [7] L. J. Cornelissen, J. Liu, R. A. Duine, J. B. Youssef, and B. J. van Wees, *Nat. Phys.* **11**, 1022 (2015).
- [8] H. Adachi, K.-i. Uchida, E. Saitoh, and S. Maekawa, *Rep. Prog. Phys.* **76**, 036501 (2013).
- [9] S. Hoffman, K. Sato, and Y. Tserkovnyak, *Phys. Rev. B* **88**, 064408 (2013).
- [10] S. M. Rezende, R. L. Rodríguez-Suárez, R. O. Cunha, A. R. Rodrigues, F. L. A. Machado, G. A. Fonseca Guerra, J. C. Lopez Ortiz, and A. Azevedo, *Phys. Rev. B* **89**, 014416 (2014).
- [11] B. L. Giles, Z. Yang, J. S. Jamison, and R. C. Myers, *Phys. Rev. B* **92**, 224415 (2015).
- [12] A. Kehlberger, U. Ritzmann, D. Hinzke, E.-J. Guo, J. Cramer, G. Jakob, M. C. Onbasli, D. H. Kim, C. A. Ross, M. B. Jungfleisch *et al.*, *Phys. Rev. Lett.* **115**, 096602 (2015).
- [13] H. Jin, S. R. Boona, Z. Yang, R. C. Myers, and J. P. Heremans, *Phys. Rev. B* **92**, 054436 (2015).
- [14] T. Kikkawa, K.-i. Uchida, S. Daimon, Z. Qiu, Y. Shiomi, and E. Saitoh, *Phys. Rev. B* **92**, 064413 (2015).
- [15] A. Kirihara, K.-i. Uchida, Y. Kajiwara, M. Ishida, Y. Nakamura, T. Manako, E. Saitoh, and S. Yoroza, *Nat. Mater.* **11**, 686 (2012).
- [16] M. Schreier, A. Kamra, M. Weiler, J. Xiao, G. E. W. Bauer, R. Gross, and S. T. B. Goennenwein, *Phys. Rev. B* **88**, 094410 (2013).
- [17] N. Vlietstra, J. Shan, B. J. van Wees, M. Isasa, F. Casanova, and J. Ben Youssef, *Phys. Rev. B* **90**, 174436 (2014).
- [18] M. Schreier, N. Roschewsky, E. Dobler, S. Meyer, H. Huebl, R. Gross, and S. T. B. Goennenwein, *Appl. Phys. Lett.* **103**, 242404 (2013).
- [19] U. Ritzmann, D. Hinzke, A. Kehlberger, E.-J. Guo, M. Kläui, and U. Nowak, *Phys. Rev. B* **92**, 174411 (2015).
- [20] S. T. B. Goennenwein, R. Schlitz, M. Pernpeintner, K. Ganzhorn, M. Althammer, R. Gross, and H. Huebl, *Appl. Phys. Lett.* **107**, 172405 (2015).